https://doi.org/10.48048/tis.2022.2077

Complex Optical Investigation of Sodium Superoxide Loaded Phosphovanadate Glass System in Ultra-Violet and Visible Region

Rajesh Barde[1,*], Kailash Nemade[2] and Sandeep Waghuley[3]

[1]Department of Physics, Government Vidarbha Institute of Science and Humanities, Amravati 444604, India
[2]Department of Physics, Indira Mahavidyalaya, Kalamb, India
[3]Department of Physics, Sant Gadge Baba Amravati University, Amravati 444602, India

([*]Corresponding author's e-mail: rajeshbarde1976@gmail.com)

Received: 18 January 2022, Revised: 2 March 2022, Accepted: 18 March 2022, Published: 10 November 2022

Abstract

Sodium superoxide loaded phosphovanadate based glass systems were prepared from a mixture of vanadium pentoxide (V_2O_5), phosphorus pentoxide (P_2O_5) boric acid (H_3BO_3) and sodium superoxide (NaO_2) using a melt-quenching method. Amorphous phase of as-prepared glass system confirmed using XRD technique. Surface morphology of glass system studied using scanning electron microscope. Ultraviolet-visible spectroscopy was employed to extract complex optical parameters like direct and indirect optical band gap, Urbach energy, refractive index, complex dielectric constant and optical conductivity. The absorption bands in the region 200 - 400 nm are recognized to the ligand-to-metal charge transfer. The region of 400 - 600 nm is ascribed to the pair excitation processes. The refractive index increases initially and then decreases for 15 and 20 mol % of NaO_2 due non bridging oxygen (NBO) atoms. The 25 mol % of NaO_2 sample shows maximum value of extinction coefficient and refractive index. The direct and indirect band gap energies vary in between 2.067 to 1.824 eV and 1.869 to 1.495 eV, respectively. With increase in concentration of NaO_2, the effective band gap of NaO_2 decreases because band edge shifted into forbidden gap due to increase in defect levels below the conduction. This primary report on sodium superoxide loaded phosphovanadate based glass systems opens wide avenue for battery and supercapacitor applications. Tailing in the bandgap was observed and found to obey Urbach rule.

Keywords: Optical properties, Sodium superoxide, Phosphovanadate glass, Optical conductivity, Urbach energy, Direct band gap, Dielectric constant

Introduction

Conducting glasses are potential candidate for solid state batteries due their admirable conductivity and chemical stability against atmospheric changes. In this category, V_2O_5 glasses has a great potential due to its advantages like generating various structural groups [1,2], showing electrical and optical properties and mostly its competence as a host for different metallic ions [3]. These properties usually used in fabrication of electrochemical batteries [4], memory switching devices [5] and supercapacitor [6]. The electrical properties of vanadate glasses are determined by the transition metal ions which existing in V^{4+} and V^{5+} states and the conduction mechanism is conquered by small polaron hopping between them [7,8]. One of the greatest imperative glass forms is Borate glass as it is often appropriate, optical and dielectric, it also insulates materials that are extremely transparent, have a low melting point and have a high thermal stability. It can also be utilized in many applications [9,10]. The B_2O_3-P_2O_5 glasses are more popular for their low refractive index and extraordinary optical properties [11]. These glasses exhibit excellent chemical durability when doped with transition metals due to formation of BO_4 tetrahedral, which transforms metaphosphate chain into 3-dimensional network [12]. Hence, they are useful as tune able solid-state lasers [13], optical materials [14], memories [15], luminescence materials [16], converters for solar energy [17] and fiber optic communication devices [18].

Now a days, sodium-ion batteries have been explored as the most promising power sources for electrical energy storage due to energy crisis and pollution from fossil fuels. [19,20]. The NaO_2 battery that takes advantage of the superoxide chemistry differentiates itself among current energy-storage techniques [21]. The sodium superoxide is feasible to the cell chemistry than lithium oxide cells, due to easily noticeable discharge products [22]. The preparation of stable superoxide is a complicated task for the researchers. Nemade *et al.* reported the novel synthesis approach for stable NaO_2. The spray pyrolysis technique is employed for preparation of NaO_2 nanoparticles in which high density oxygen environment is

maintain to achieve higher degree of purity in superoxide phase [23]. These batteries can be cycled forming sodium superoxide as the lone discharge product with improved cycle life [24]. Peled *et al.* reported that using sodium as the anode and oxygen as the cathode, these batteries ran several cycles at the temperature of 105 °C [25]. Hartmann *et al.* reported that a sodium superoxide battery with 0.2 V voltage polarizations upon charge, which makes this technology as optimistic competitor to lithium oxygen batteries. The results of the study show that sodium superoxide crystals forms in a one-electron allocation step as a solid discharge. This work opens the way for the replacement of lithium-ion by sodium for batteries, which offer an unpredicted outcome as metal-air batteries [22]. These batteries have engrossed great attention because they exhibit the highest theoretical energy density while also offering the advantages of elemental earth abundance and potential cost efficiency [26]. The photochromic effect enticed many researchers. The main defect found in the glasses arenNegative electron-centers (EC) and positive hole. This defect was investigated by optical spectroscopy to inspect their electronic transitions that cause high absorbance in the UV-VIS region [27]. Thakur *et al.* studied the optical, structural, and dielectric spectroscopic properties of B2O3-Bi2O3 glasses glasses doped with ZrO2, and SeO2 which confirms the ionic character of the studied glass samples [28].

In this we plan to investigate the complex optical properties of sodium superoxide doped vanadate glass system in UV and visible region. Several parameters like as optical band gap, Urbach energy, refractive index, complex dielectric constant and optical conductivity were investigated at room temperature.

Materials and methods

NaO_2 was synthesis from AR grade, SD fine sodium nitrate ($NaNO_3$) by heating in oxygen rich surrounding [29]. For the preparation of glasses 99 % Purity, SD fine vanadium pentoxide (V_2O_5), phosphorus pentoxide (P_2O_5) and boric acid (H_3BO_3) along with a prepared NaO_2 was used. The samples of compositions $60V_2O_5$–$5P_2O_5$–(35-x) B_2O_3–xNaO_2, x = 5, 10, 15, 20 and 25 mol % were prepared by usual melt-quenching method as described in our previous work [30]. By using Bruker D8 advance with Cu Kα radiation the phase purity and structure of as prepared NaO_2 and glasses were confirmed with scan rate 6.00 in the range 20° - 80°. Morphologies of all prepared samples were studied by using JEOL-6390LV SEM. Ultraviolet-visible spectro-photometer was used to record the optical properties of all prepared glasses, from which the optical band gap, Urbach energy, refractive index, Complex dielectric constant and optical conductivity were calculated.

Results and discussion

XRD pattern of NaO_2 is shown in **Figure 1**. The peaks (200), (220), (311) and (222) appear in XRD accurately index to NaO_2 according to JCPDS reference card No. 01-077-0207, which confirms the formation of NaO_2 [22, 29]. In XRD pattern of prepared glass samples depicts in **Figure 2**, there was no characteristic peak which corresponds to any crystalline phase pointed out the formation of glasses.

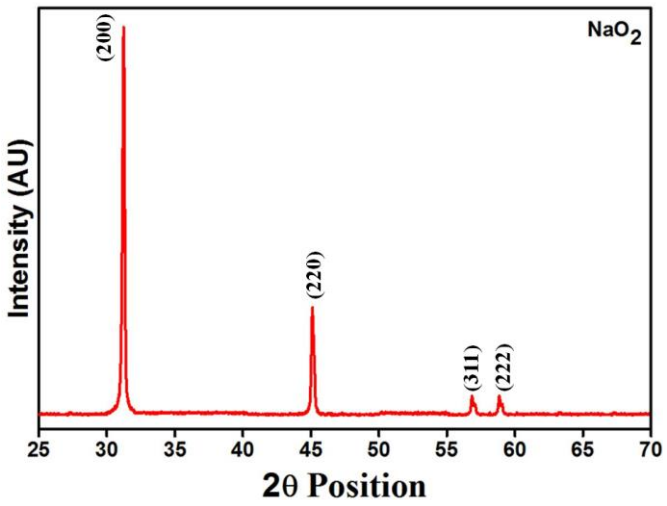

Figure 1 XRD of Sodium Superoxide (NaO_2).

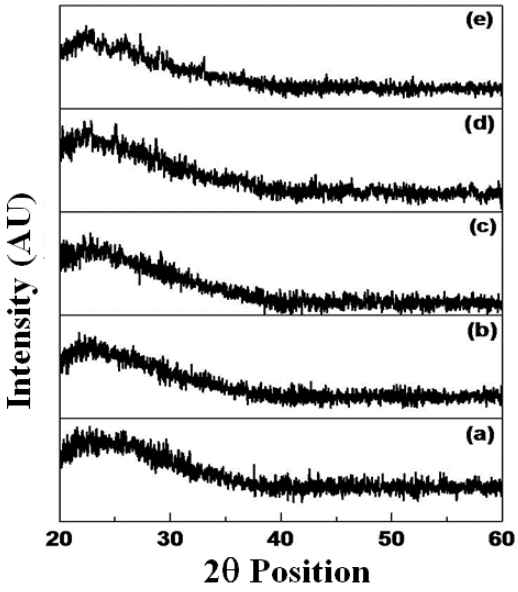

Figure 2 XRD of $60V_2O_5–5P_2O_5–(35\text{-}x)B_2O_3–xNaO_2$ for (a) 5 mol %, (b) 10 mol %, (c) 15 mol %, (d) 20 mol % and (e) 25 mol % of NaO_2.

From **Figure 3** it is shows that, the grains are high agglomerated having good interconnectivity between the particles, which helps the transportation of charge particles [31]. From the image it is clear that sample exhibit an irregular granular morphology.

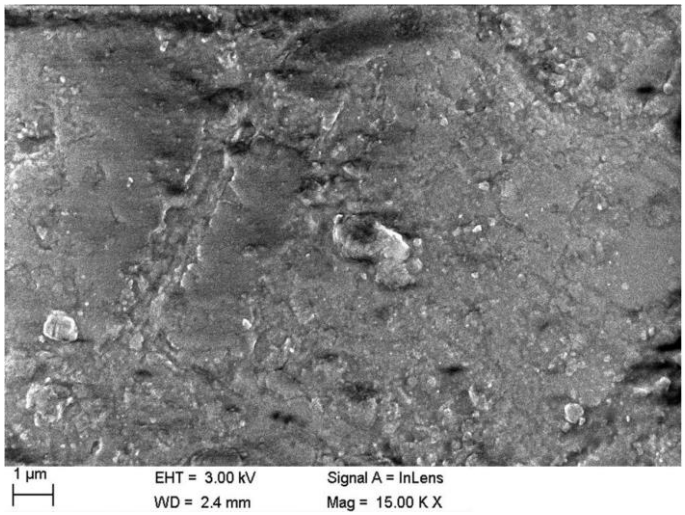

Figure 3 SEM image of 20 mol % of NaO_2 doped glass sample.

The absorption spectra were recorded at room temperature by using UV-Visible spectrophotometer in range of 200 - 600 nm. From the absorbance, the optical absorption coefficient (α) was calculated. After correction for reflection losses, α may be find out by using the relation [32]:

$$\alpha(\vartheta) = \frac{2.303\,A}{l} \quad (1)$$

where *l* is the sample thickness in cm and A is defined by A = log (Io/I) where Io and I are the intensity of the incident and transmitted beams.

From these spectra, displayed in **Figure 4**, shows an intense absorption dip in the wavelength region 220 to 230 nm and a broad hump in the wavelength region of 300 - 450 nm. The absorption bands in the region 200 - 400 nm are recognized to the ligand-to-metal charge transfer [33]. The region of 400 - 600 nm is ascribed to the pair excitation processes [34]. The broad absorption band between 250 - 450 nm may be due to the charge transfer transition from O_2^- to Na^+ in NaO_2.

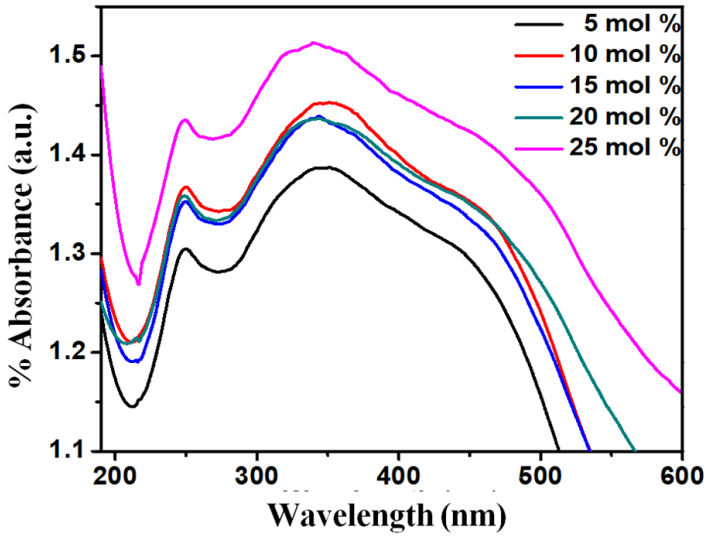

Figure 4 Absorption spectra of the glass systems.

The optical properties of as such prepared glass system may be represented by the refractive index (n) and extinction coefficient (k), which are the real and imaginary components of the complex refractive index $N = n - ik$, respectively. The extinction coefficient can be estimated by using the relation [35];

$$k = \frac{\alpha\lambda}{4\pi} \quad (2)$$

where, α is % absorption and λ is wavelength.

From **Figure 5(a)** shows that, in the region 225 - 500 nm, extinction coefficient of all glasses increases linearly and it is measure of capturing of light, which concluded that light trapping is proportional to wavelength. The extinction coefficient curve becomes almost linear beyond 525 nm. [36,37]. Which is favourable with absorption behavior of glass system. The 25 mol % of NaO_2 sample shows maximum value of extinction coefficient.

Refractive index has an important role in the search for optical materials, in optical communication and in designing antireflection coating [38]. The refractive index was estimated using the formula Eq. (3) [36];

$$n = \frac{1}{\%\,T} + \sqrt{\frac{1}{\%\,T} - 1} \quad (3)$$

where %T is transmission through sample.

Figure 5(b) shows the plot of refractive index with wavelength, which shows that samples have jagged reduction in refractive index around 225 nm due to strong absorption in UV region. Also, samples have small value of refractive index on shorter wavelength side, whereas on longer wavelength side its value increases up to 340 nm and beyond it, refractive index decreases gradually. With the concentration of NaO_2, refractive index also increases initially and then decreases for 15 and 20 mol % of NaO_2 due non bridging oxygen (NBO) atoms. The maximum value of refractive index is detected for 25 mol % of NaO_2.

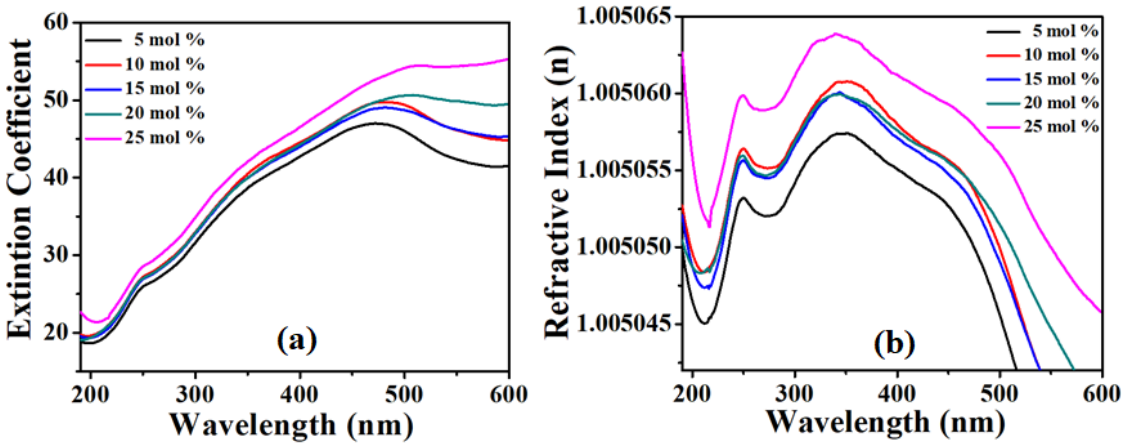

Figure 5 (a) Variation of extinction coefficient and (b) Variation of refractive index of the glass system as a function of wavelength.

Analysis of absorption spectra is one of the most valuable means for explaining the optical transition and electronic band structure materials. The band gap is also very important properties for photovoltaic device application. The basic principle is that, electromagnetic wave interacts with the electron in valance band and photon having higher energy than the band gap will be absorbed. There are 2 categories of optical transitions direct and indirect and in both cases, due to interaction of electromagnetic waves with electrons in the valence band, it raised across the fundamental gap and goes to the conduction band. The expression of the absorption co-efficient, (α) to determine direct and indirect band gap (Eg) was given by Davis and Mott [39]:

$$\alpha h\vartheta = A\left(h\vartheta - E_g\right)^m \quad (4)$$

where A is an energy dependent constant, Eg is the optical band gap of the material, m is a constant that depends on the semiconducting materials, which can be expected to have values of 1/2, 3/2, 2 and 3. The value of m depends on the type of the electronic transition responsible for absorption; 1/2 for allowed direct transitions, for direct forbidden transitions it is 3/2, for allowed indirect transitions it is 2 and for indirect forbidden transitions it is 3 [23]. For glassy materials indirect transitions (m = 2) are valid according to the Tauc's relations. The indirect optical energy band gaps (Eg') of samples can be found by plotting $(\alpha h\upsilon)^{1/n}$ verses hυ and extrapolating it to $(\alpha h\upsilon)^{1/n} = 0$.

Figures 6(a) and **6(b)** shows the Tauc plots for indirect and direct band gap energy of different composition of NaO_2 loaded glass system, respectively. The direct and indirect band gap energies vary in between 2.067 to 1.824 eV and 1.869 to 1.495 eV respectively. The band gap of the glasses became more and more narrower along with the concentration of NaO_2. Also, due to increase in NaO_2 in the glasses creates a large number of donor centers and growth of new polaronic can lead to a considerable reduction in the band gap which suggests the conversion of the bridging oxygen (BO) atoms in to non-bridging oxygen (NBO) in the glasses. The band gap of glasses are effectively impacts as NBOs have higher energies than the BOs. The addition of NaO_2 may increases localized electrons due to increase of donor center in the which decreases the band gap and it is accountable for the red shift of the absorption edge [40]. It indicated that NaO_2 doping successfully extended their solar response spectra.

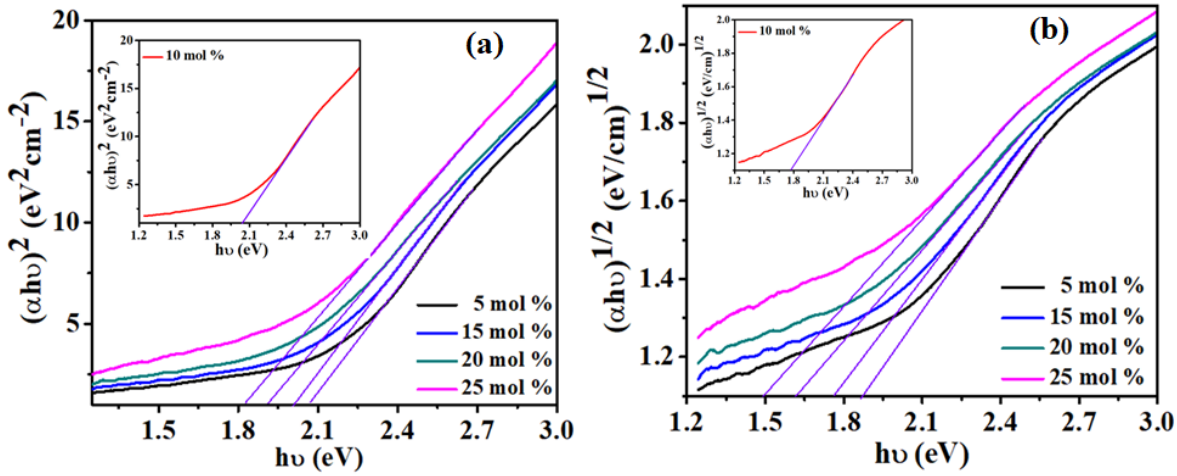

Figure 6 (a). Tauc plot of $(\alpha h\upsilon)^2$ versus photon energy and (b) Tauc plot of $(\alpha h\upsilon)^{1/2}$ versus photon energy of various glass samples.

The width of the defect bands formed in the band gap of NaO_2 as an intermediate state which create a band tail known as the Urbach tail on both sides of the top of the valence band and bottom of the conduction band and the energy associated with this tail is referred as Urbach energy explained by following equation;

$$\alpha(\vartheta) = \alpha_0 exp\left(\frac{h\vartheta}{E_U}\right) \quad (5)$$

where α_0 is a constant, hυ is the photon energy and E_U is the Urbach's energy [41,42].

The E_U is calculated from the plot of Ln α vs. hυ, i.e., from the slopes of the linear portion, below the band gap and the source of it is considered as thermal vibrations in the lattice. Urbach energy for each glass samples are as shown in **Figure 7** which varies in between 0.433 to 0.574 eV. The defect energy increases with decrease in band gap, which obviously supports the creation of sub-band states in between the valence and conduction bands consequence in the reduction of the band gap. With increase in concentration of NaO_2, the effective band gap of NaO_2 decreases because band edge shifted into forbidden gap due to increase in defect levels below the conduction [43, 44]. The relationship of the band gap with Urbach energy for different samples are shown in **Figure 8(a)**. The pictorial representation of formation of Urbach tail in NaO_2 doped V_2O_5–P_2O_5–B_2O_3 glass is shown in **Figure 8(b)**. **Table 1** displays the estimated values of direct, indirect band gap and Urbach energies for various NaO_2 contents.

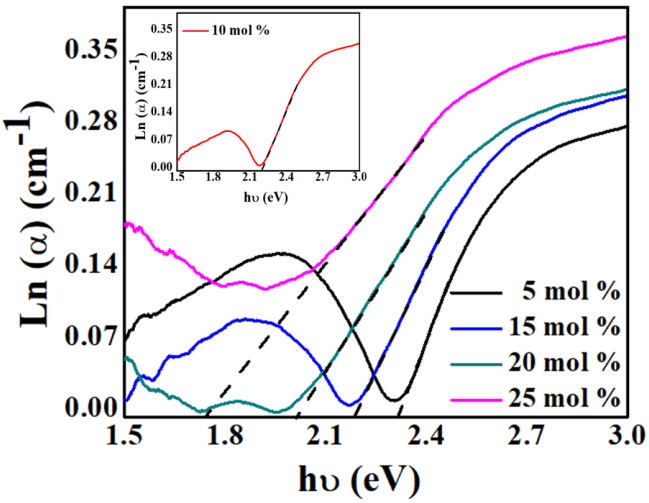

Figure 7 Plot of Ln(α) vs. hυ for the determination of Urbach energy.

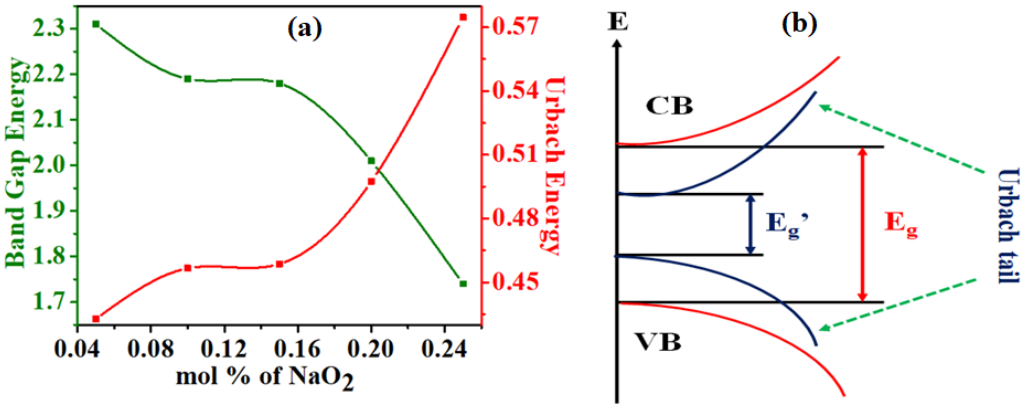

Figure 8 (a) Variation of band gap and Urbach energy for different mol % of NaO_2. and (b) Formation of Urbach tail for NaO_2 doped V_2O_5–P_2O_5–B_2O_3 glass.

Table 1 Direct, indirect band gap values and the Urbach energies for various NaO_2 contents.

Sample	Direct band gap Energy (E_g) (eV)	Indirect band gap Energy ($E_{g'}$) (eV)	Urbach Energy (E_U) (eV)
5 mol %	2.067	1.869	0.433
10 mol %	2.407	1.771	0.456
15 mol %	2.008	1.762	0.459
20 mol %	1.912	1.618	0.497
25 mol %	1.824	1.495	0.575

The optical dielectric function is complex quantity which consists of real part (ε_r) which represents the ability of materials to reduce speed of light and imaginary part (ε_i) represents absorption of energy from an electric field respectively. Both part of dielectric constant shows direct relation with refractive index (n) and extinction coefficient (k) [45,46].

$$\varepsilon_r = n^2 - k^2 \quad (6)$$

$$\varepsilon_i = 2nk \quad (7)$$

It is found that ε_r mostly depended on n^2 because of insignificant values of k^2, while ε_i mostly depends on k values which are related to the change of absorption coefficients.

The plots of real and imaginary part of dielectric constant verses wavelength at room temperature are shown in **Figure 9(a)** and **9(b)**, respectively. The value of ε_r increases linearly with wavelength from 225 nm up to 490 nm. The 25 mol % of NaO_2 sample shows uppermost value of ε_r, hence it exhibits highest ability to slowdown light, as real dielectric constant is measure of slowdown of speed of light [47]. The curve of ε_i increases linearly from 225 nm upto 500 nm. In this, due to dipole motion, 25 mol % of NaO_2 sample have the highest strength to absorb energy from an electric field. [48]. In this both real and imaginary parts follow the same pattern and ε_r are higher than the ε_i.

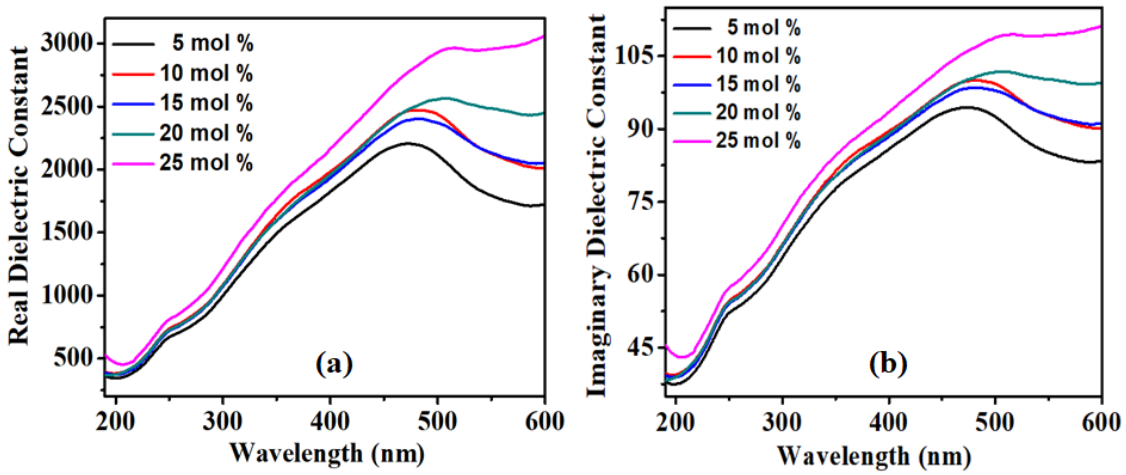

Figure 9 (a) Variation of real dielectric constant and (b) Variation of imaginary dielectric constant as a function of wavelength.

Optical conductivity denotes the optical response of a material and the dimension is same as that of frequency which is valid solitary in a Gaussian system. The optical conductivity (σ_{opt}) has been calculated by using the relation [37],

$$\sigma_{opt} = \frac{\alpha cn}{4\pi} \quad (8)$$

where c, α and n are speed of light, absorption coefficient and the refractive index respectively. The plot of σ_{opt} with photon energy is shown in **Figure 10**. It shows that σ_{opt} increases with photon energy as well as NaO_2, which may be due to the increase of both absorption coefficient and refractive index with NaO_2 also due to the change in density of localized states in band gap [49,50], and electron excited by photon energy.

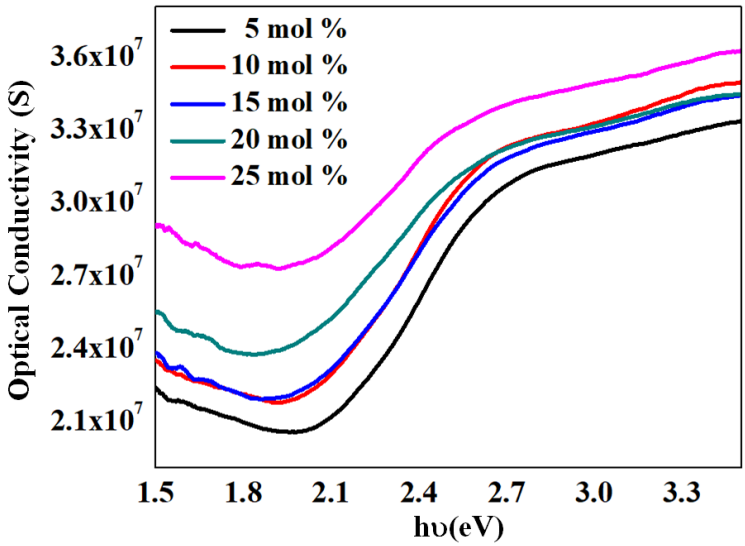

Figure 10 Variation of optical conductivity of glass samples as a function of photon energy.

Conclusions

The present work successfully reports the preparation of sodium superoxide loaded phosphovanadate glass system by melt-quenching method. The prepared glass system has good quality amorphous phase, confirmed through XRD study. The absorption spectra show intense absorption dip in the wavelength region 220 to 230 nm and a broad hump in the wavelength region of 300 - 450 nm. The prepared glass system shows capturing of light that is extinction coefficient is proportional to wavelength in range 225 - 500 nm. Prepared samples have small value of refractive index on shorter wavelength side, whereas on longer wavelength side its value increases up to 340 nm and beyond it, refractive index decreases gradually. The values of direct and indirect band gap, and Urbach energy were successfully estimated for the prepared glass system. The dielectric constant measurements show linear behavior with wavelength. The defect energy increases with decrease in band gap, which obviously supports the creation of sub-band states in between the valence and conduction bands consequence in the reduction of the band gap. With increase in concentration of NaO_2, the effective band gap of NaO_2 decreases because band edge shifted into forbidden gap due to increase in defect levels below the conduction.

Acknowledgements

The author acknowledges Director, Government Vidarbha Institute of Science and Humanities, Amravati, Head, Department of Physics, Government Vidarbha Institute of Science and Humanities, Amravati, and Head, Department of Physics, Sant Gadge Baba Amravati University, Amravati for providing necessary facilities for the work.

References

[1] GI Petrov, VV Yakovlev and J Squier. Raman microscopy analysis of phase transformation mechanisms in vanadium dioxide. *Appl. Phys. Lett.* 2002; **81**, 1023-5.
[2] MM El-Desoky and MS Al-Assiri. Structural and polaronic transport properties of semiconducting $CuO–V_2O_5–TeO$ glasses. *Mater. Sci. Eng. B* 2007; **137**, 237-46.
[3] GM Clark and AN Pick. DTA study of the reactions of V_2O_5 with metal (II) oxides. *J. Therm. Anal.* 1975; **7**, 289-300.
[4] H Liu and D Tang. Synthesis of ZnV_2O_6 powder and its cathodic performance for lithium secondary battery. *Mater. Chem. Phys.* 2009; **114**, 656-9.
[5] E Mansour, YM Moustafa, GM El-Damrawi, SA El-Maksoud and H Doweidar. Memory switching of $Fe_2O_3–BaO–V_2O_5$ glasses. *Physica B* 2001; **305**, 242-9.
[6] K Jeyalakshmi, S Vijayakumar, S Nagamuthu and G Muralidharan. Effect of annealing temperature on the supercapacitor behaviour of β-V_2O_5 thin films, Mater. *Res. Bull*. 2013; **48**, 760-6.
[7] L Murawski. Electrical conductivity in iron-containing oxide glasses. *J. Mater. Sci.* 1982; **17**, 2155-63.
[8] NF Mott. Conduction in glasses containing transition metal ions. *J. Non-Cryst. Solids* 1968; **1**, 1-17.
[9] MA Hassan, FM Ebrahim, MG Moustafa, ZMA El-Fattah and MM El-Okr. Unraveling the hidden Urbach edge and Cr^{6+} optical transitions in borate glasses. *J. Non Cryst. Solids* 2019; **515**, 157.
[10] AI Ismail, A Samir, F Ahmad, LI Soliman and A Abdelghany. Spectroscopic studies and the effect of radiation of alkali borate glasses containing chromium ions. *J. Non Cryst. Solids* 2021; **565**, 120743.
[11] S Yusub and D Krishna Rao. The role of chromium ions on dielectric and spectroscopic properties of $Li_2O–PbO–B_2O_3–P_2O_5$ glasses. *J. Non-Cryst. Solids* 2014; **398-399**, 1-9.
[12] RK Brow and DR Tallant. Structural design of sealing glasses, J. Non-Cryst. *Solids* 1997; **222**, 396-406.
[13] TO Hardwell. *Solid-state lasers: Properties and applications*. Nova Science Pub Inc, New York, 2008, p. 227.
[14] B Denker, B Galagan, V Osiko, S Sverchkov and E Dianov. Luminescent properties of Bi-doped boro-alumino-phosphate glasses. *Appl. Phys. B* 2007; **87**, 135-7.
[15] O Mao, RL Turner, IA Courtney, BD Fredericksen, MI Buckett, LJ Krause and JR Dahn. Active/inactive nanocomposites as anodes for Li-Ion batteries. *Electrochem. Solid-State Lett.* 1999; **2**, 3-5.
[16] CR Kesavulu, RPS Chakradhar, RS Muralidhara, JL Rao and RV Anavekar. EPR, optical absorption and photoluminescence properties of Cr^{3+} ions in lithium borophosphate glasses. *J. Alloys Compd.* 2010; **496**, 75-80.

[17] JT Tsai, CY Huang and ST Lin. The development of conductive pastes for solar cells. *Adv. Mater. Res.* 2012; **557- 559**, 1201-4.

[18] JW Yu and K Oh. New in-line fiber band pass filters using high silica dispersive optical fibers. *Opt. Commu.* 2002; **204**, 111–8.

[19] F Li, Z Wei, A Manthiram, Y Feng, J Maa and L Maid. Sodium-based batteries: From critical materials to battery systems. *J. Mater. Chem. A* 2019; **7**, 9406-31.

[20] X Xu, KS Hui, DA Dinh, KN Hui and H Wang. Recent advances in hybrid sodium-air batteries, *Mater. Horiz.* 2019; **6**, 1306-35.

[21] X Ren and Y Wu. A low-overpotential potassium-oxygen battery based on potassium superoxide. *J. Am. Chem. Soc.* 2013; **135**, 2923-6.

[22] P Hartmann, CL Bender, M Vracar, A Garsuch, AK Durr, J Janek and P Adelhelm. A rechargeable room-temperature sodium superoxide (NaO2) battery. *Nat. Mater*. 2012; **12**, 228-32.

[23] KR Nemade and SA Waghuley. Novel synthesis approach for stable sodium superoxide (NaO_2) nanoparticles for LPG sensing application. *Int. Nano Lett.* 2017; **7**, 233-6.

[24] M He, KC Lau, X Ren, N Xiao, WD McCulloch, LA Curtiss and Y Wu. Concentrated electrolyte for the sodium-oxygen battery: Solvation structure and improved cycle life. *Angew. Chem. Int. Ed*. 2016; **55**, 1-6.

[25] E Peled, D Golodnitsky, H Mazor, M Goor and S Avshalomov. Parameter analysis of a practical lithium- and sodium-air electric vehicle battery. *J. Powe. Sour.* 2011; **196**, 6835-40.

[26] H Park, J Kim, MH Lee, SK Park, D Kim, Y Bae, Y Ko, B Lee and K Kang. Highly durable and stable sodium superoxide in concentrated electrolytes for sodium-oxygen batteries. *Adv. Energy Mater.* 2018; **8**, 1801760.

[27] MS Sadeq and MA Abdo. Effect of iron oxide on the structural and optical properties of alumino-borate glasses. *Ceram. Int.* 2021; **47**, 2043-9.

[28] S Thakur, A Kaur and L Singh. Mixed valence effect of Se^{6+} and Zr^{4+} on structural, thermal, physical, and optical properties of B_2O_3–Bi_2O_3–SeO_2–ZrO_2 glasses. *Opt. Mat.* 2019; **96**, 109338.

[29] RV Barde. Preparation, characterization and CO_2 gas sensitivity of polyaniline doped with sodium superoxide. *Mater. Res. Bull.* 2016; **73**, 70-6.

[30] RV Barde and SA Waghuley. Preparation and electrical conductivity of novel vanadate borate glass system containing graphene oxide. *J. Non-Cryst. Solids* 2013; **376**, 117-25.

[31] RV Barde and SA Waghuley. Transport properties of rare earth CeO_2 doped phospho-vanadate glass systems. *J. Chin. Adv. Mater. Soc.* 2014; **2**, 273-83.

[32] M Fox. *Optical properties of solids*. Oxford University Press, New York, 2001, p. 274.

[33] JB Lian, XC Duan, JM Ma, P Peng, T Kim and WJ Zheng. Hematite (alpha-Fe_2O_3) with various morphologies: Ionic liquid-assisted synthesis, formation mechanism, and properties. *ACS Nano* 2009; **3**, 3749-61.

[34] T Wang, S Zhou, C Zhang, J Lian, Y Liang and W Yuan. Facile synthesis of hematite nanoparticles and nanocubes and their shape-dependent optical properties. *J. Chem*. 2014; **38**, 46-9.

[35] S Gedia, V Reddy, M Reddya, C Parkb, JC Wookb and KTR Reddy. Comprehensive optical studies on SnS layers synthesized by chemical bath deposition. *Opti. Mate.* 2015; **42**, 468-75.

[36] RV Barde. Influence of CeO_2 content on complex optical parameters of phosphovanadate glass system, Spectroch *Spectrochim. Acta A Mol. Biomol. Spectrosc.* 2016; **153**, 160-4.

[37] RV Barde, KR Nemade and SA Waghuley. Complex optical study of V_2O_5–P_2O_5–B_2O_3–GO glass systems by ultraviolet-visible spectroscopy. *Opti. Mate*. 2015; **40**, 118-21.

[38] KL Chopra and I Kaur. *Thin film phenomena*. McGraw-Hill, New York, 1969, p. 736.

[39] S Song, Y Wang, X Yuan, W Yao, W Jing. Characterization and preparation of Sn-doped CuGaS2 thin films by paste coating. *Mater. Lett.* 2015; **148**, 41-4.

[40] S Shailajha, K Geetha, P Vasantharani and SPSA Kadhar. *Spectrochi. Acta Part A: Mole. and Biomol. Spectro.* 2015; **138**, 846-56.

[41] K Boubaker. A physical explanation to the controversial Urbach tailing universality. *Eur. Phys. J. Plus* 2011; **126**, 10.

[42] B Choudhur, B Borah and A Choudhury. Extending photocatalytic activity of TiO_2 nanoparticles to visible region of illumination by doping of cerium. *Photochem. Photobiol.* 2012; **88**, 257-64.

[43] B Choudhury, M Dey and A Choudhury. Defect generation, d-d transition, and band gap reduction in Cu-doped TiO2 nanoparticles. *Int. Nano Lett*, 2013; **3**, 1-8.

[44] CO Ayieko1, RJ Musembi, SM Waita, BO Aduda and PK Jain. Structural and optical characterization of nitrogen-doped TiO_2 thin films deposited by spray pyrolysis on fluorine doped tin oxide (FTO) coated glass slides. *Int. J. Ene. Eng.* 2012; **2**, 67-72.

[45] AQ Abdullah. Surface and volume energy loss, optical conductivity of rhodamine 6G dye (R6G), *Chem. and Mat. Res.* 2013; **3**, 56-63.
[46] RV Barde, KR Nemade and SA Waghuley. Complex optical study of V_2O_5–P_2O_5–B_2O_3–Dy_2O glass systems. *J. Taib. Uni. Sci.* 2015; **10**, 340-4.
[47] P Sharma and SC Katyal. Determination of optical parameters of a-(As2Se3)90Ge10 thin film. *J. Phys. D: Appl. Phys.* 2007; **40**, 2115-20.
[48] NA Bakr, AM Funde, VS Waman, MM Kamble, RR Hawaldar, DP Amalnerkar and SR Jadkar, Determination of the optical parameters of a-Si: H thin films deposited by hot wire-chemical vapour deposition technique using transmission spectrum only. *Pramana J. Phys.* 2011; **76**, 519-31.
[49] NF Mott and EA Davis. Conduction in non-crystalline systems V conductivity, optical absorption and photoconductivity in amorphous semiconductors. *Philos. Mag.* 1970; **22**, 0903-22.
[50] F Yakuphanoglu, A Cukurovali and I Yilmaz. Refractive index and optical absorption properties of the complexes of a cyclobutane containing thiazolylhydrazone ligand. *Opt. Mater.* 2005; **27**, 1363-8.